Petroleum Science 19 (2022) 2830–2843

Contents lists available at ScienceDirect

Petroleum Science

journal homepage: www.keaipublishing.com/en/journals/petroleum-science

Original Paper

New insight into fracturing characterization of shale under cyclic soft stimulation: A lab-scale investigation

Qiang Gao [a, c], Han Cao [a, b, c], Ting Bao [e], Jiang-Zhan Chen [d, *], Huan-Xiao Hu [a, c], Ping-He Sun [a, c, **]

[a] School of Geoscience and Info-Physics, Central South University, Changsha, 410083, Hunan, China
[b] Hubei Intelligent Geological Equipment Engineering Technology Research Center, Wuhan, 430074, Hubei, China
[c] Key Laboratory of Metallogenic Prediction of Nonferrous Metals and Geological Environment Monitoring (Ministry of Education), Central South University, Changsha, 410083, Hunan, China
[d] School of Resources and Safety Engineering, Central South University, Changsha, 410083, Hunan, China
[e] Pacific Northwest National Laboratory, Richland, WA, 99352, USA

ARTICLE INFO

Article history:
Received 12 February 2022
Received in revised form
27 July 2022
Accepted 6 August 2022
Available online 11 August 2022

Edited by Yan-Hua Sun

Keywords:
Cyclic soft stimulation
Fracturing mechanical characterization
Damage evolution
Crack extending criterion
Radiated energy

ABSTRACT

The cyclic soft stimulation (CSS) is a new method of reservoir reforming for which the mechanism of fracturing crack propagation is ambiguous with regard to the alternating fluid pressure. This study aims to provide a comprehensive understanding of the fracturing mechanical characterizations of CSS under different magnitudes and amplitudes of the alternating fluid pressure. Acoustic emission (AE) is recorded to investigate the damage evolution under CSS based on the *b* value analysis of AE. Experimental results reveal the difference of pressure in a crack under different cyclic fluid pressure conditions. The AE results show that the maximum radiated energy under CSS tends to be reduced with the increase in the amplitude and magnitude of the alternating fluid pressure. The finishing crucial touch is that the crack extending criterion under CSS is proposed, which combines the injection parameters, the rock properties and *in-situ* stress. According to the crack extending criterion, the fluctuation fluid pressure causes the reduction of a critical crack extending pressure, and the CSS causes the crack to initiate and propagate under low fluid pressure. Under a higher-value magnitude of alternating fluid pressure, the cyclic times of CSS is less for the crack initiation. In supplement to the crack extending criterion, a distinct relationship between the radiated energy and the cyclic fluid pressure also is established based on the energy dissipation criterion. These new findings provide an insight into the determination of crack extending criterion under CSS for efficiently implementing shale fracturing.

1. Introduction

Conventional energy resources play a vital role in supplying the energy demand around the world (McGlade, 2012). Efficient mining of unconventional energy has typically striven to resolve the energy crisis. Hydraulic fracturing has been applied to stimulate the unconventional reservoir to strengthen the productivity and mobility of shale gas (Mateusz et al., 2019; Tan et al., 2020). The process of the fluid injection is associated with an interaction between the fracturing fluid and formation (Ali et al., 2018; Chen et al., 2019; Huang et al., 2019; Zhuang et al., 2019; Lei et al., 2020), as a result, the pore distribution of formation is changed. Further, the stress field presents dynamic, and the propagation of cracks (direction, width and height, etc.) is complex. The conventional hydraulic fracturing is to continuously inject fluids with a constant rate to generate fractures in target formations. With the stress attenuation around cracks, a large amount of stimulated energy is released under the action of tensile and shear stress (Ingrid and Marte, 2017; Wang et al., 2022). Severely, the radiated energy can induce micro seismic in the tectonic areas such as fault distribution zone, etc. Previous works (Bao and Eaton, 2016; James and Verdon, 2016; Lee et al., 2019; Antonio et al., 2020) have shown that the interaction

* Corresponding author.
** Corresponding author. School of Geoscience and Info-Physics, Central South University, Changsha, 410083, Hunan, China.
E-mail addresses: jiangzhanchen@csu.edu.cn (J.-Z. Chen), pinghesun@csu.edu.cn (P.-H. Sun).

https://doi.org/10.1016/j.petsci.2022.08.003

Nomenclature

a	Half-width of crack, mm
A_i	Amplitude of AE event
A_{min}	Minimum amplitude of AE events in each time window
b	AE analytical parameters
C	Half-length of crack, mm
D	Damage variable
e	Natural logarithm base
e_{eff}	Effective energy during the CSS, mV ms
e_{tot}	Total input energy, mV ms
K_I	Stress intensity factor of the "I" type crack, MPa $m^{1/2}$
K_{IC}	Fracture toughness of the "I" type crack, MPa $m^{1/2}$
$L(\Delta t)$	Fluid migration length in Δt time, m
n	Total number of AE events in each window
N	Time cycles of pressurization and depressurization
Δp	Hydraulic pressure variation, MPa
P_c	Critical crack extending pressure, MPa
P_{extend}	Extending pressure acting on the crack by fluid injection, MPa
P_f	Injected flow pressure, MPa
$P_{initiate}$	Crack initiation pressure, MPa
P_w	Fluid pressure, MPa
$P(x, t)$	Fluctuating fluid pressure, MPa
ΔQ	Volume of fluid, m^3/s
R	Equivalent radius of fractured segment, m
t	Flow time, s
$u(x, t)$	Flow velocity, m/s
U_s	Surface energy, mV ms
U_s'	New surface energy under CSS, mV ms
x	Coordinate, m
α	Biot coefficient
γ	Surface energy in unit
γ'	New surface energy in unit under CSS
μ	Viscosity coefficient, mPa s
ρ_0	Fluid density, g/cm^3
σ_1	Axial stress, MPa
σ_3	Confining stress, MPa
σ_t	Tensile strength of rock, MPa

between hydraulic fracturing and formation will significantly interfere with the *in-situ* stress causing the fault activation, the dislocation of the earth's crust, and the destabilization of the bottom layer, even the generation of micro-earthquakes. These studies claim that the magnitude of micro-earthquakes is linked to the maximum radiated energy of hydraulic fracturing. As the major problem caused by unconventional energy exploitation, the microseismic has aroused global thinking, which brings non-resource and non-technical troubles to many unconventional energy-producing areas (Lee et al., 2019).

For unconventional reservoir fracturing, the current issue is how to reduce the possible micro-earthquake caused by hydraulic fracturing. Some scholars referred to the cyclic stimulation in the enhanced geothermal systems (EGS) (Zimmermann et al., 2010, 2015; Philip et al., 2020) and presented the cyclic soft stimulation (CSS) (Bai et al., 2006; Zang et al., 2013; Hofmann et al., 2019). Moreover, the CSS is accomplished by adjusting the fluid rate or fluid pressure to stimulate the formation. This will make the crack initiation pressure and maximum radiated energy reduction, thus avoiding a bigger magnitude of micro-seismic. To emphasize the advantage of cyclic stimulation, there are many comparisons (Bai et al., 2006; Diaz et al., 2018b; Liang et al., 2018a; Hofmann et al., 2019; Lou and Zhang, 2019; Chao et al., 2020; Xie et al., 2020; Wu et al., 2020) between cyclic hydraulic fracturing (CHF) and monotonic hydraulic fracturing (MHF). In these works, hydraulic fracturing tests focus on cubic granite and sandstone specimens. And that, about 80% of crack initiation pressure was assumed as the peak value of the alternating fluid pressure to investigate the influence of CHF (Patel et al., 2017; Diaz et al., 2018a); Farkas et al. (2018); Hofmann et al. (2018); Liang et al. (2018b); Zhuang et al. (2018); Zhou et al. (2019) and the minimum value of the alternating fluid pressure closes to zero. It is important to study the impact of the amplitude of the cyclic fluid pressure on the hydraulic fracturing results. Moreover, in the process of fluid pressure reduction, the micro-cracks will be closed under the *in-situ* stress. Therefore, the study of the effective fluid pressure magnitude of cyclic stimulating is urgent for unconventional reservoir exploration.

Shale is an unconventional gas reservoir with the characteristics of low permeability and low porosity (Chen et al., 2017b; Cao et al., 2020). Therefore, in the process of hydraulic fracturing, the change of the fluid pressure and the injection rate presents a consistent trend in shale (Fig. 1). However, the fluid pressure is cyclically fluctuating between two pressure values (P_1, P_2) in the CHF, the coupling of the alternating fluid pressure and the formation has a great influence on the initiation and propagation of cracks. On the one hand, the fluid state is different under varied pressure. It is necessary to understand the mechanism of interaction between different amplitudes and magnitudes of alternating fluid pressure and the formation, further to clear the threshold of the alternating fluid pressure for shale gas exploitation. But a few works in the literature consider the low cyclic fluid pressure of CHF in shale. On the other hand, the duration of the fluid invading in CHF is

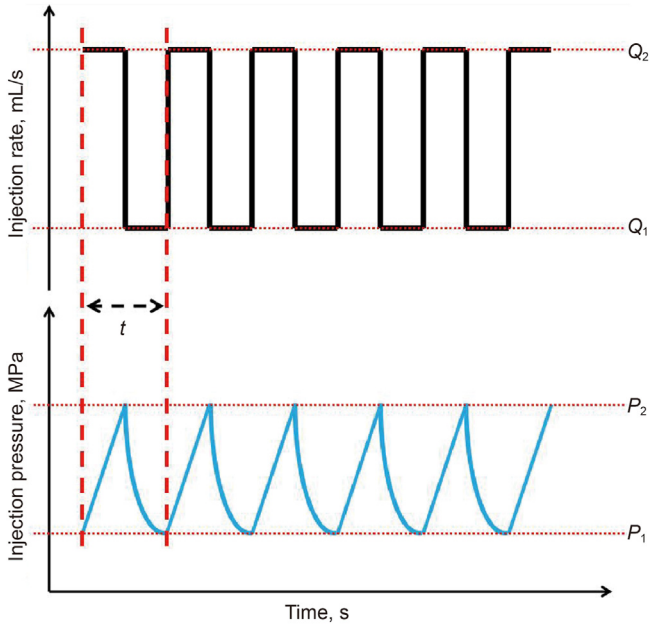

Fig. 1. Change of fluid injection rate and fluid pressure in the tight reservoir (modified from Zang et al., 2019).

generally longer than that in MHF. With a long period of fluid-solid coupling, the formation will perform different mechanical characteristics. Therefore, it is important to investigate the effect of cyclic soft stimulating (CSS) on shale gas exploitation.

In this paper, first, different magnitudes and amplitudes of CSS were conducted in shale-like samples, then the fluid pressure and the crack propagation are discussed. To understand the mechanism of fracturing crack propagation under CSS, the damage evolution and a crack extending criterion were obtained. Finally, the maximum radiated energy during the sample breaking was studied. The novelty is that we comprehensively investigate the impact of different ranges of cyclic fluid pressure on the crack propagation of shale and the maximum radiated energy of fracturing. The crucial touch is that the crack extending criterion under CSS is proposed, which combines the injection parameters, the rock properties and *in-situ* stress. These new findings provide an insight into the determination of crack extending criterion under CSS for efficiently implementing shale fracturing.

2. Materials and methods

2.1. Test equipment

The equipment used in the test is the self-developed device for hydraulic fracturing under triaxial loading (Fig. 2a), which is composed of three parts: a loading system, a fluid injection system, and a monitoring system. (1) The loading system: both the maximum confining and axial loading are 50 MPa. The suitable specimen for the equipment is the cylinder with a diameter of 100 mm and a height of 190–210 mm. The axial loading disks have a round hole with a diameter of 8 mm in the center. The fluid injection pipe is connected to the fluid container through the round hole. (2) The injection system: the maximum pressure of the injection system is 40 MPa, and the rate range is 0–10 mL/min with an accuracy of 0.01 mL/min. (3) The monitoring system includes the fluid pressure monitoring part, the confining stress monitoring part, and the acoustic emission (AE) monitoring part, which can get the radiated energy during crack propagating. To accurately collect the AE parameters, the piezoelectric element of the AE sensor is the chip composed of the lead zirconate titanate and ceramic. In the process of CSS, six AE sensors were applied to monitor the elastic wave and the radiated energy of fracturing. Both the layout of AE sensors and the loading distribution are shown in Fig. 2b. The acquisition frequency of the AE system was 16 kHz, the threshold value of data collection was set as 30 mV, and the gain multiple of the pre-amplifier was selected as 40 dB.

2.2. Test materials

To eliminate the influence of the bedding in shale and guarantee the repeatability of the results, the shale-like cylindrical samples (Fig. 3) with a diameter of 100 mm and a height of 200 mm were prepared based on the similarity principle. On account that the mechanical mechanism of hydraulic fracturing and the cyclic soft stimulation is a more significant topic, the bedding of shale was not considered in detail in this investigation. The samples applied in this investigation were described in detail in previous literatures (Chen et al., 2019; Gao et al., 2019). The shale-like cylindrical samples are homogeneous, and the fracturing mechanical characterizations and the radiated energy are the major research object, which is beneficial to studying the influence of CSS on hydraulic fracturing. In the testing, the sample was connected to the injection system through an injection pipe with an outer diameter of 4 mm and an inner diameter of 2 mm. The naked segment is located in the middle of the sample with a length of 60 mm. The fracturing fluid used in the test is distilled water. To understand the impact of cyclic soft stimulation, two sets of samples were tested in terms of the amplitude of cyclic stimulation and the magnitude of fluid pressure.

2.3. Test procedure

The test procedure consists of three steps. First, the triaxial stresses were applied with axial stress of 5 MPa and initial confining stress of 4 MPa. For the effect of true triaxial stress on the results, some works have been conducted in previous literature (Gao et al., 2019). Second, the monotonic hydraulic fracturing (MHF) with an injection rate of 10 mL/min was conducted to obtain the fracturing characteristic of cracks, including crack initiation pressure, crack propagation pressure, break pressure and crack

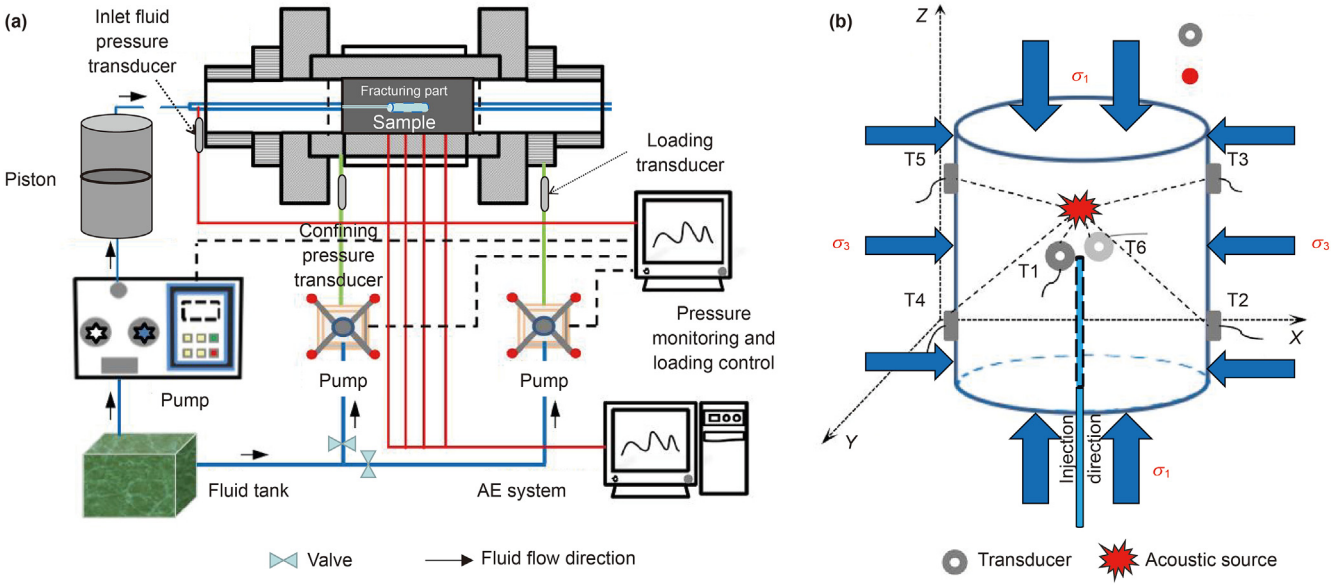

Fig. 2. (**a**) Cyclic fracturing experimental system; (**b**) Layout of AE sensors and loading distribution.

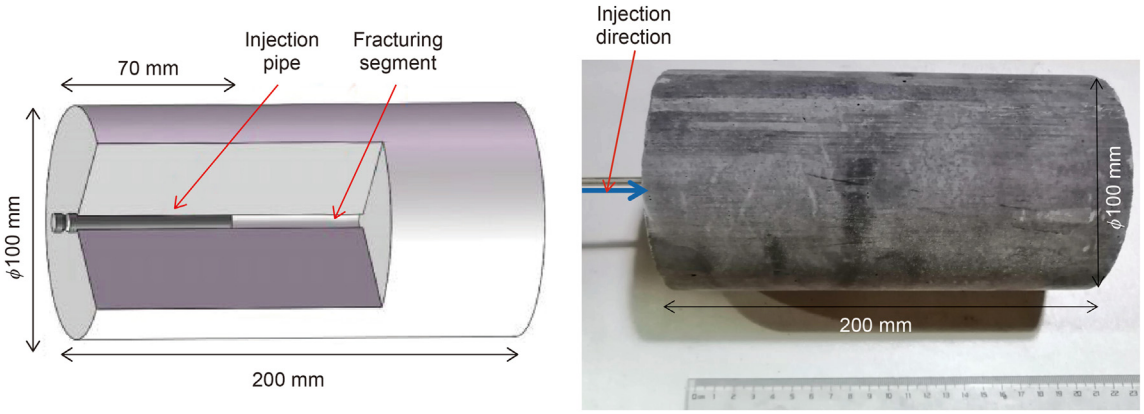

Fig. 3. Experimental sample.

intersecting pressure in the fluid pressure curve. Third, based on the fluid pressure curve of MHF, the amplitudes and magnitudes of alternating fluid pressure in CSS were determined (Table 1 and Fig. 4a). For the amplitudes of alternating fluid pressure in CSS, the samples were divided into a test group with an amplitude of 2 MPa and a test group with an amplitude of 4 MPa. For the magnitudes of alternating fluid pressure in CSS, the lower-value and the higher-value fluid pressure were confirmed. Then, the different ranges of CSS were conducted. Where, the duration of cyclic fluid injection is 1 h and the injection rate changed between 10 and 0.5 mL/min (refer to Fig. 4b) to produce the alternating fluid pressure. In the process of CSS, the alternating fluid pressure is dependent on the experimental scheme in Table 1. Finally, the fluid pressure was increasing with an injection rate of 10 mL/min until the sample was broken down.

3. Results

3.1. Monotonic hydraulic fracturing (MHF)

For the analysis of the experimental results in cyclic soft stimulation, different stages and fracturing parameters under MHF are discussed. The results of the fluid pressure are shown in Fig. 5. It can be seen that the fluid pressure curve of MHF is composed of the stages of pressurization, crack initiation, crack propagation, sample break, and crack interacting until the fluid injection is stopped. There is a significant decline in the fluid pressure once the sample is broken, which indicates that at the initial stage of the crack interacting, the fluid pressure variation of the sample is formed by hydraulic fracturing, and the sample is broken down with the tensile failure mode (Fig. 5). Finally, the cracks intersect the wall of the sample, the fluid pressure increases due to the rubber boundary in the cyclic fracturing experimental system. Therefore, the fluid pressure has an obvious change in different stages under MHF, and the results will be researched further in the cyclic soft stimulation.

3.2. Cyclic soft stimulation (CSS)

Based on the results in Section 3.1, Fig. 6a shows the fluid pressure under lower-value magnitude CSS. With the increase in the amplitude of CSS, the duration of crack propagation decreases significantly under the lower-value magnitude of cyclic fluid pressure. It indicates that the fracture process zone under alternating fluid pressure of large amplitude is wider than that of small amplitude. Therefore, with the given diameter of the sample, the duration of crack propagation is reduced. On the condition that the magnitude of CSS increases, the similar results can be obtained (Fig. 6a and b). The duration of crack interacting increases with the increase in the alternating amplitude or magnitude. The reason is that the larger the alternating amplitude or magnitude of fluid pressure is, the wider the fracture process zone of the sample will be, thus increasing the interaction path and the interaction time. Therefore, it can be concluded that the fracture process zone increases obviously under a large amplitude or magnitude of fluid pressure.

The fluid pressure curve in high magnitude CSS can be divided into two stages (Fig. 7): uniform and non-uniform cyclic changes. For the uniform cyclic change, the change of fluid pressure is linear, but with the action of alternating fluid pressure, the non-uniform cyclic change presented owing to the fracture process. Compared with the lower-value magnitude of cyclic fluid pressure (Fig. 7a), the highlight is the significant reduction in fluid pressure fluctuations during the crack propagation under the higher-value magnitude of cyclic fluid pressure (Fig. 7c), and the higher-value magnitude CSS strengthens the fracture process zone and increases the continuity of crack interaction paths caused by

Table 1
Test scheme parameters.

Amplitude of cycles	Sample	Magnitude of fluid pressure	Range of cyclic pressure, MPa
\	S01	\	Direct
2	S02	Lower-value	0–2
	S06	Lower-value	1–3
	S03	Higher-value	6–8
4	S04	Lower-value	0–4
	S07	Higher-value	5–9
	S05	Higher-value	6–10

Note: Sample S01 was used for the monotonic hydraulic fracturing. In the process of the experiment, we carried out monotone hydraulic fracturing, different amplitudes, and magnitudes of alternating fluid pressure three times, respectively.

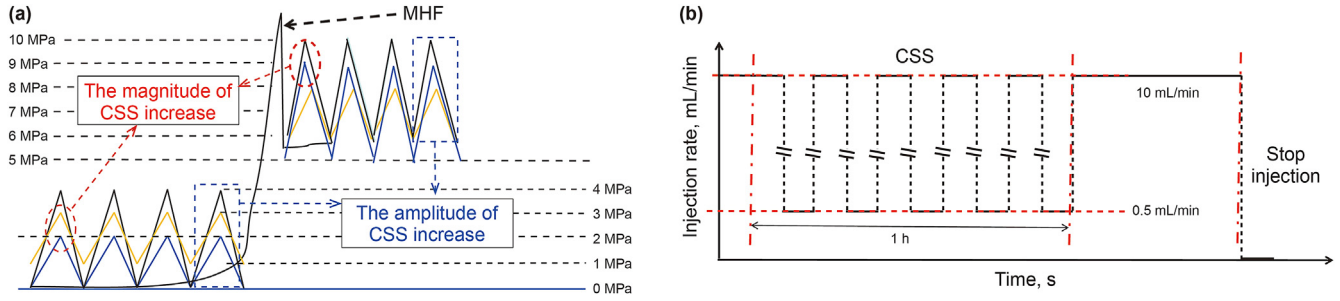

Fig. 4. (**a**) Sketch of testing; (**b**) Injection rate in the testing.

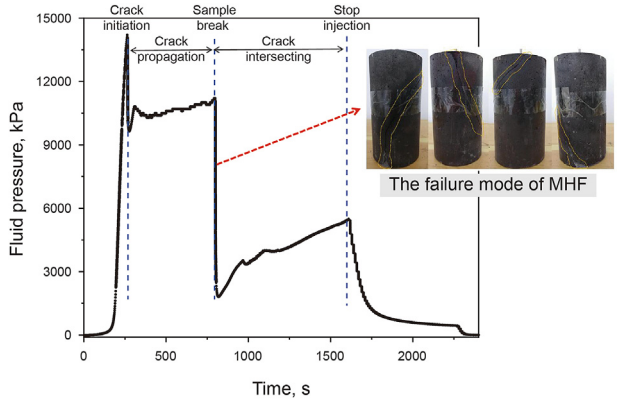

Fig. 5. Fluid pressure under MHF.

fracturing. This can be reflected by the reduction of pressurization rate under higher-value magnitude alternating fluid pressure in the process of circulating fluid injection (Fig. 7c). In particular, the crack initiation and the break of the sample almost occurred at the same time under the higher-value magnitude of CSS. Therefore, the fracture process zone of the higher-value magnitude of alternating fluid pressure is significantly wider, and the time interval between the crack initiation and the break of the sample reduces. As a result, there is almost no crack propagation. Therefore, the higher-value alternating fluid pressure promotes the increment of the fracture process zone. Moreover, as shown in Fig. 7a and b, with the amplitude of CSS increases, the duration of crack propagation decreases, and the fluctuation of fluid pressure during crack interacting increases, it can infer that the deformation of the sample increases owing to the propagation of cracks.

3.3. Peak value of fluid pressure

The peak value is an important parameter of fracturing characterization, and it shows the crack initiation. As shown in Fig. 8 and Table 2, the smaller the magnitude of CSS, the larger the peak value of fluid pressure, which shows that the fracture process zone is less under the lower-value magnitude of alternating fluid pressure, and the sample is fractured in CSS with high crack initiation pressure. However, with the higher-value magnitude of CSS, the peak value of fluid pressure is small because the fracture process zone is large. As the amplitude of CSS increases, the peak value of fluid pressure is decreased obviously, and the stimulation of a larger amplitude of cyclic fluid pressure significantly increases the fracture process zone of the samples. Therefore, with the increase in circulation amplitude, the peak value of fluid pressure decreases significantly.

Based on the theoretical overview of hydraulic fracturing, the crack initiation pressure around the pilot hole can be calculated according to the Kirsch equation as follows (Sampath et al., 2018):

$$P_{\text{initiate}} = 3\sigma_3 - \sigma_1 + \sigma_t - \alpha P_w \tag{1}$$

In the testing, the value of crack initiation pressure (P_{initiate}) is equal to the peak value of the fluid pressure. Based on the fluid mechanics theory (You, 2015; Tong and Gao, 2018a, 2018b), the motion equation of the non-monotonous fluid in a homogeneous fractured segment is:

$$\rho_0 \frac{\partial u(x,\ t)}{\partial t} + \frac{\partial P(x,\ t)}{\partial x} = 0 \tag{2}$$

Compared with MHF, multiple fluid injections and pressure reduction are added in the CSS process. The frequent pressurization and depressurization of fluid pressure will produce fatigue damage; in this stage, the fluid volume with the stable flow is as follows (Chen et al., 2017a):

$$\Delta Q = \frac{\Delta p}{L(\Delta t)} \frac{\pi}{8\mu} R^4 \tag{3}$$

Therefore, the flow rate of non-monotonous in the homogeneous fractured segment is:

$$u(x,\ t) = \frac{\Delta Q}{\pi R^2} = \frac{1}{8\mu} \frac{\Delta p R^2}{L(\Delta t)} \tag{4}$$

The internal fluid pressure in the pilot hole often fluctuates in the fracturing process. The fluctuation has an impact on the peak value of the fluid pressure. Therefore, the research process is an ideal fracturing process, and the fluctuating pressure of the fluid is obtained by combining Eq. (4) and Eq. (2) as:

$$P_{(x,\ t)} = M \cdot \Delta p \cdot x \cdot \frac{\partial L(\Delta t)}{L^2(\Delta t)\partial t} \tag{5}$$

with

$$M = \frac{\rho_0 R^2}{8\mu} = 9.16 \times 10^{-2}$$

Then, the injected flow pressure (P_f) in the cracks is composed of the fluctuating fluid pressure ($P_{(x,\ t)}$) and the fluid pressure (P_w), which can be expressed as:

$$P_f = P_{(x,\ t)} + P_w = 9.16 \times 10^{-2} \cdot \left(x \cdot \frac{\partial L(\Delta t)}{L^2(\Delta t)\partial t} \right) \cdot \Delta P + P_w \tag{6}$$

When $P_f - P_{\text{initiate}} > 0$, the crack is propagating. Combining Eq. (1) and Eq. (6), it is deduced:

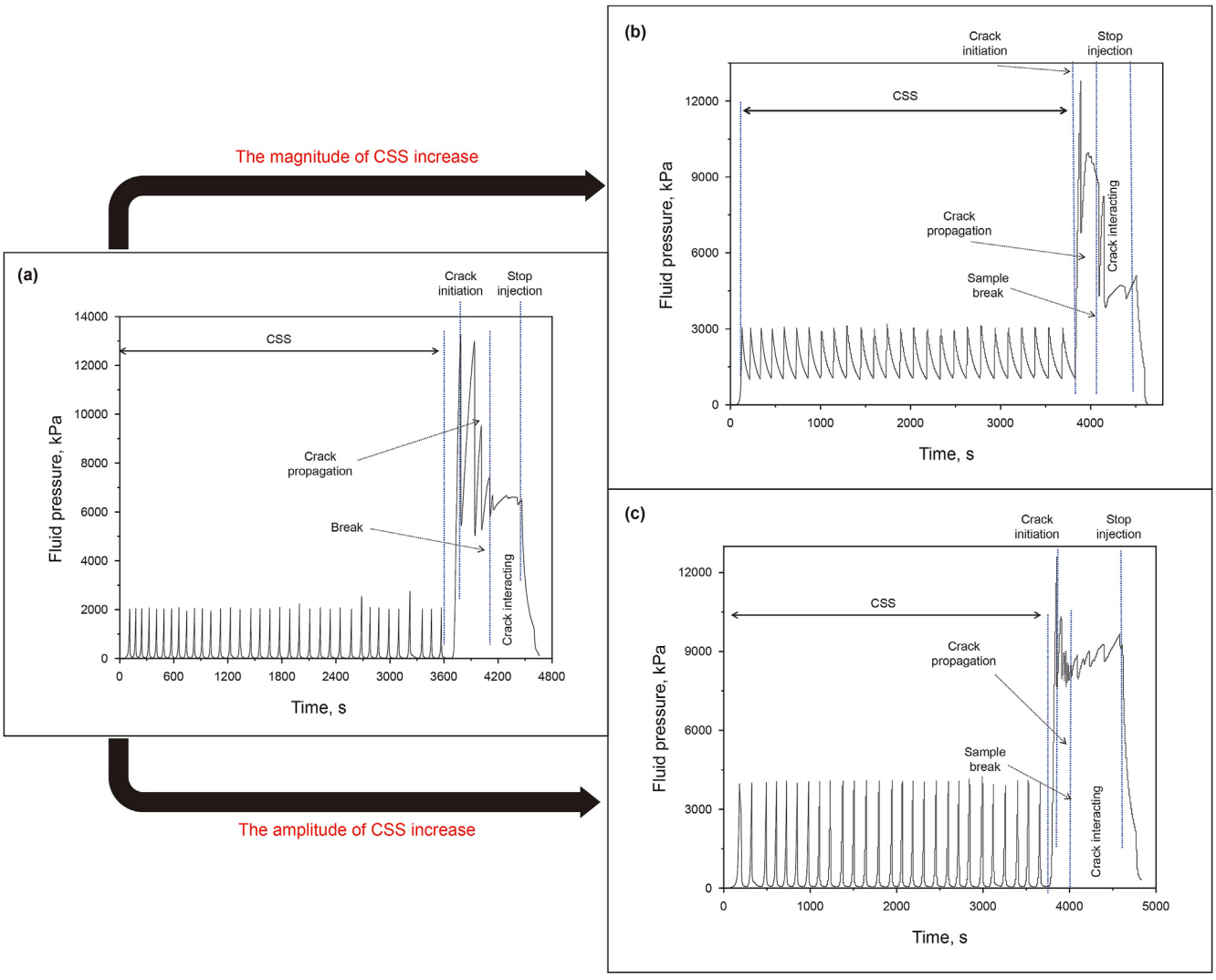

Fig. 6. Fluid pressure with different magnitudes and amplitudes of CSS under low fluid pressure.

$$P_f - P_{initiate} = 9.16 \times 10^{-2} \cdot \left(x \cdot \frac{\partial L(\Delta t)}{L^2(\Delta t)\partial t} \right) \cdot \Delta P + (1+\alpha)P_w - (3\sigma_3 - \sigma_1 + \sigma_t) > 0 \quad (7)$$

According to Eq. (7), with the increase in fluid pressure (P_w) and the amplitude (ΔP) of CSS, the P_f increases owing to the fracture process enlarging the porosity of the sample. Therefore, the peak value of the fluid pressure will reduce, and the crack initiation pressure will be decreased, but the injected flow pressure P_f is increased under CSS. In particular, under higher-value magnitude fluid pressure (P_w) and large amplitude cyclic fluid pressure (ΔP), it is confirmed that P_f is greater than $P_{initiate}$. As a result, the crack initiates easily.

3.4. Propagation pressure and propagation rate

The crack propagation under the CSS can be used to characterize the strength of the skeleton around the cracks, and the propagation pressure and the propagation rate are the characteristic fracturing parameters (Cao et al., 2021). Fig. 9a shows that with the increase in the magnitude or amplitude of alternating fluid pressure, the pressurization rate and the propagation pressure of the crack under the CSS increase. It concludes that the strength of the skeleton around cracks is reduced under the CSS, but for the skeleton non-contacted with fluid, its strength increases because of the compaction of the fluid pressure (Cao et al., 2021). Thus, the pressurization rate and the average fluid pressure of crack propagation under the CSS increase obviously. However, under the action of higher-value magnitude CSS, the cracks have been completely propagated, and the sample breaks down in the stage of cyclic fluid pressure stimulation. Therefore, with the increase in the pressurization rate, the low values of fluid pressure indicate that the skeleton at the front of the crack is compacted and strengthened, while the higher magnitude of alternating fluid pressure promotes the effect of the fracture process significantly and the crack propagation increases obviously.

In order to further compare the fracture process zone under different alternating fluid pressure stimulation, the durations of pressurization and crack propagation after the action of different CSS are analyzed. The larger the amplitude or the magnitude of alternating fluid pressure, the shorter the durations of pressurization and crack propagation. The fracture process zone of the sample is related to the magnitude and amplitude of the fluid pressure in

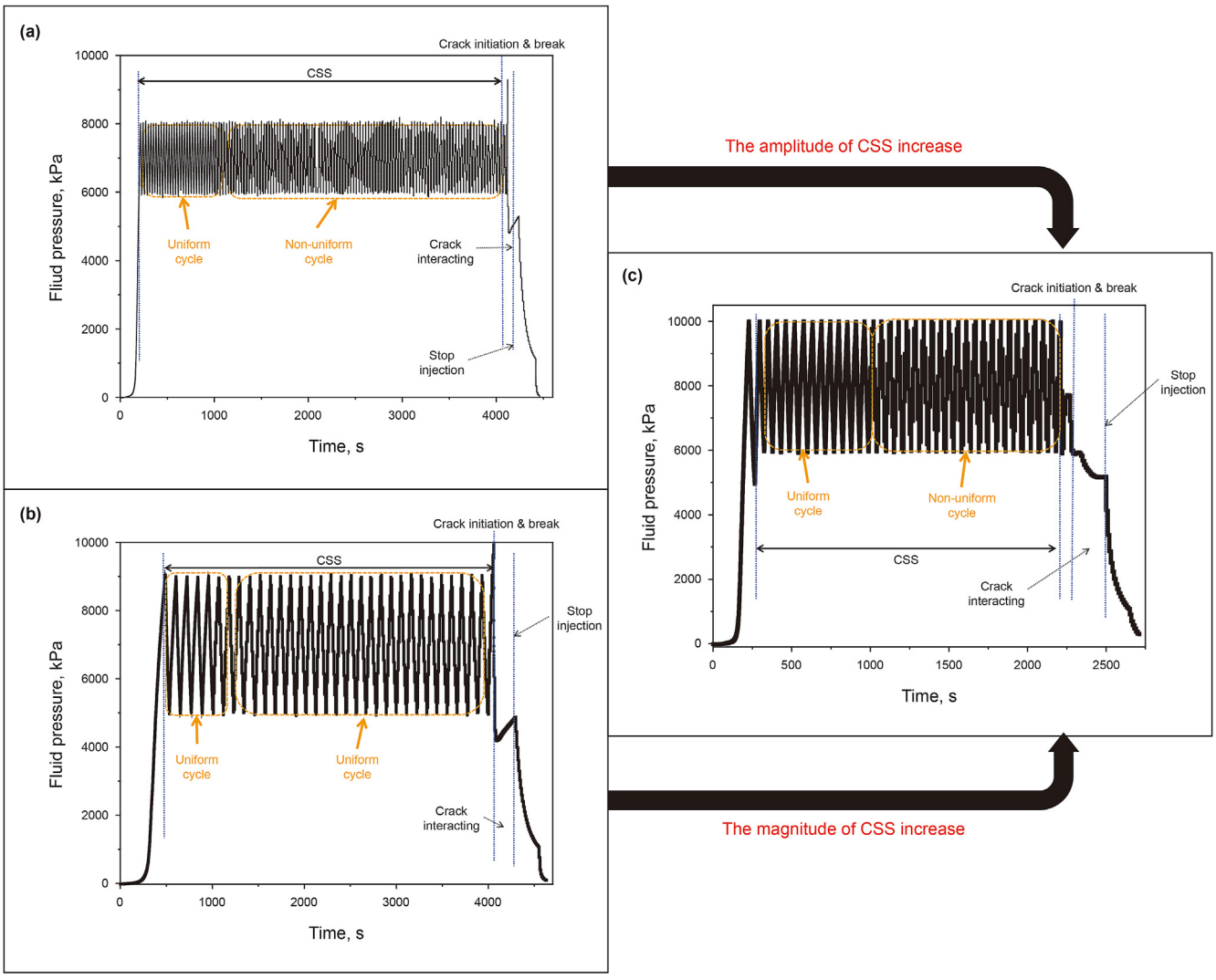

Fig. 7. Fluid pressure with different magnitudes and amplitudes of CSS under high fluid pressure.

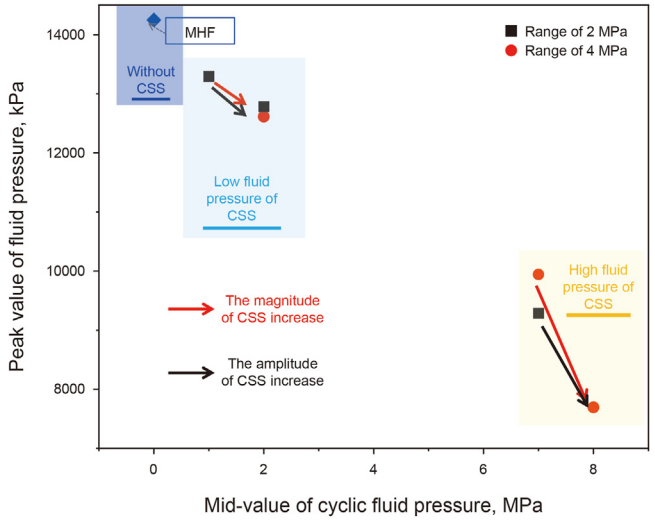

Fig. 8. Peak value of fluid pressure under MHF and the peak value of fluid pressure under different magnitudes and amplitudes of CSS.

Table 2
Peak value of fluid pressure.

Range of cyclic pressure, MPa	Peak value of fluid pressure, kPa
MHF	14247.331
0–2	13294.024
1–3	12782.463
6–8	9286.954
0–4	12613.412
5–9	9943.242
6–10	7695.134

the CSS. The greater the magnitude and amplitude of the fluid pressure, the wider the fracture process zone and the shorter the pressurization and the crack propagation. As shown in Fig. 9b with a black arrow line, on the condition that the amplitude of the CSS is the same, with the increase in the cyclic fluid pressure, the duration of the crack propagation decreases under the lower-value magnitude CSS. This shows that the fracture process zone is strongly influenced by alternating fluid pressure. In addition, the crack can propagate rapidly under the high-value magnitude CSS, leading to the sample's break, so the propagation duration is concise under this condition.

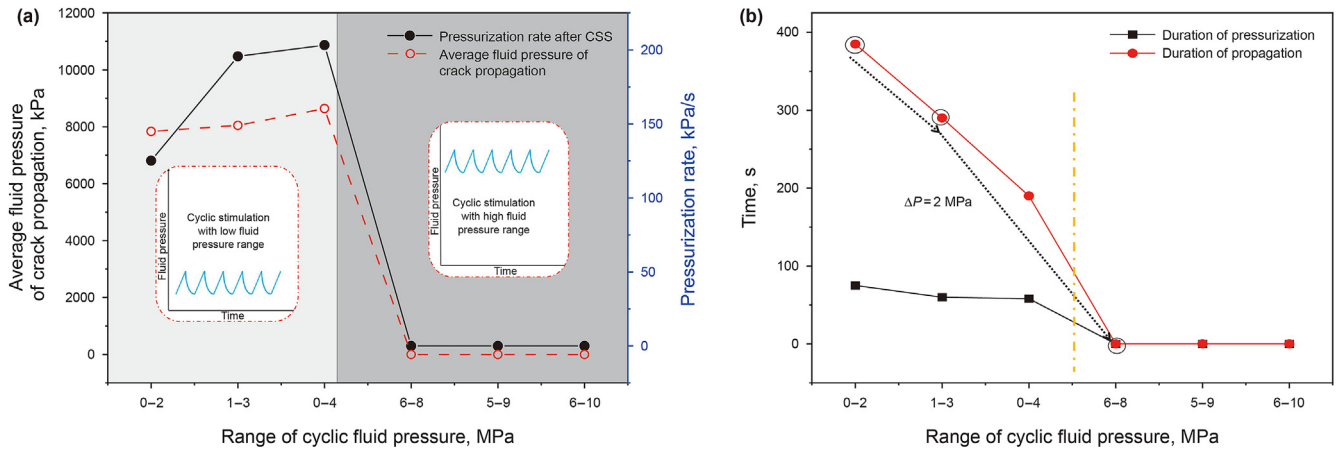

Fig. 9. (**a**) Propagation pressure and pressurization rate of the crack under different magnitudes and amplitudes of alternating fluid pressure; (**b**) Durations of pressurization and crack propagation under different magnitudes and amplitudes of CSS.

3.5. Crack extending criterion (P_{extend} and K_I) under CSS

Based on the linear elastic superposition principle (LESP) (Atkinson et al., 1992), the stress intensity factor around the crack (Fig. 10a) is represented by the superposition of stress intensity factors caused by various simple loads (Fig. 10b), that is:

$$K_I\left(\sigma_3,\ P_{(x,\ t)},\ P_w\right) = 2K_I(\sigma_3) + K_I\left(P_{(x,\ t)}\right) + K_I(P_w) \tag{8}$$

On the condition that there is only the stress σ_3, the stress intensity factor is:

$$K_I(\sigma_3) = -\sigma_3 \cdot \sqrt{R} \cdot f_{(b)} \tag{9}$$

with

$$f_{(b)} = -2\left[\left(b^2-1\right)\Big/\pi b^7\right]^{1/2}$$

$$b = 1 + a/R$$

On the condition that there is only fluid pressure, the stress intensity factor is:

$$K_I(P_w) = P_w \cdot \sqrt{R} \cdot h_{(b)} \tag{10}$$

On the condition that there is only the fluid fluctuating pressure, the stress intensity factor is:

$$K_I\left(P_{(x,\ t)}\right) = \sum_{i=1}^{N}\left(P_{(x,\ t)} \cdot \sqrt{R} \cdot g_{(b)}\right) \tag{11}$$

where $g(b)$ and $h(b)$ are determined by the change of the fluid pressure (Atkinson et al., 1992).

Then, based on the fracture criterion (Lemaitre and Desmorat, 2005), cracks begin to extend when the stress intensity factor reaches the fracture toughness. The criterion can be expressed as follows:

$$K_I\left(\sigma_3,\ P_{(x,\ t)},\ P_w\right) \geq K_{IC} \tag{12}$$

where K_{IC} is the rock fracture toughness, it is a property of rock.

Therefore, the critical crack extending pressure P_c under N time cycles of pressurization and depressurization (Atkinson et al., 1992) can be calculated as follows:

$$P_c = \frac{1}{Ng_{(b)} + h_{(b)}}\left(\frac{K_{IC}}{\sqrt{R}} + 2 \cdot \sigma_3 \cdot f_{(b)}\right) \tag{13}$$

According to the fracture mechanics and the results in Section 3.3, the extending pressure P_{extend} acting on the crack by the fluid injection is (Fig. 11):

$$P_{extend} = 9.16 \times 10^{-2} \cdot \left(x \cdot \frac{\partial L(\Delta t)}{L^2(\Delta t)\partial t}\right) \cdot \Delta P + (1+\alpha)P_w - 3\sigma_3 + \sigma_1 \tag{14}$$

When $P_{extend} > P_c$, the crack is extending, that is:

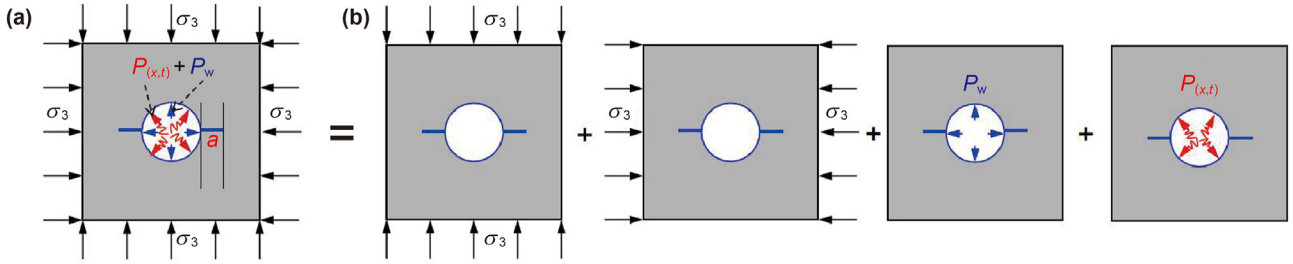

Fig. 10. Fracture model under one cyclic soft stimulation.

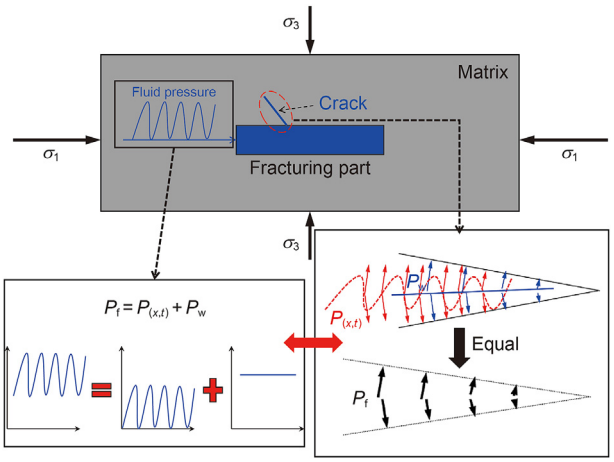

Fig. 11. Pressure on the crack under the action of pressurization and depressurization.

$$(1+\alpha)P_w + 9.16\times10^{-2}\cdot\Delta P\cdot x\cdot\frac{\partial L(\Delta t)}{L^2(\Delta t)\partial t} > (3\sigma_3-\sigma_1) + \frac{1}{Ng_{(b)}+h_{(b)}}\left(\frac{K_{IC}}{R}+2\cdot\sigma_3\cdot f_{(b)}\right) \quad (15)$$

Eq. (15) is the crack extending criterion under CSS, the left side of the Eq. (15) is composed of the injected circulating fluid parameters under CSS, and the right side is related to the rock properties and *in-situ* stress.

According to Eq. (15), the fluctuation fluid pressure ($P_{(x,\ t)}$) causes the reduction of critical crack extending pressure (P_c). The reason is that $h_{(b)}$ decreases the value of P_c, and then the P_c will gradually reduce with the increase in the cycles (n). Further, with the action of CSS, the skeleton is weakened by the alternating fluid pressure, resulting in the decrease in the fracture toughness (K_{IC}) of the sample, which indicates that the CSS causes the crack to initiate and propagate under low fluid pressure. Based on the extending pressure (P_{extend}) acting on the crack (Eq. (14)) and the critical pressure (P_c) required for the crack extending (Eq. (13)), with the increase in fluid pressure (P_w) and the amplitude (ΔP) of the fluctuating pressure, P_{extend} is larger than P_c under fewer cycles (n) of CSS, the apparent results are present in Fig. 9. Under higher-value magnitude of alternating fluid pressure, the times (n) of CSS is less for the crack initiation, it can be supported by the graphs and curves in Figs. 6 and 7. Therefore, the crack extending criterion is a critical basis for promoting the abundant propagation of cracks under CSS. For the field, on the condition that the injection cycles are sufficient, the injection fluid pressure and the amplitude of the fluctuating pressure can be reduced. As the depth increases, the *in-situ* stress is larger, and the fluid pressure or the amplitude of fluctuating pressure should be increased.

4. Discussion

4.1. Effect of CSS on the law of crack's damage evolution

To research the crack propagation and the damage evolution in the process of CSS, the acoustic emission (AE) data and the fluid pressure curves were discussed together in this part. As we all know that a small fraction of seismic energy can be captured by the AE sensors during the stress damaging and crack propagating. Therefore, the *b* value, which is an AE analytical parameter, can

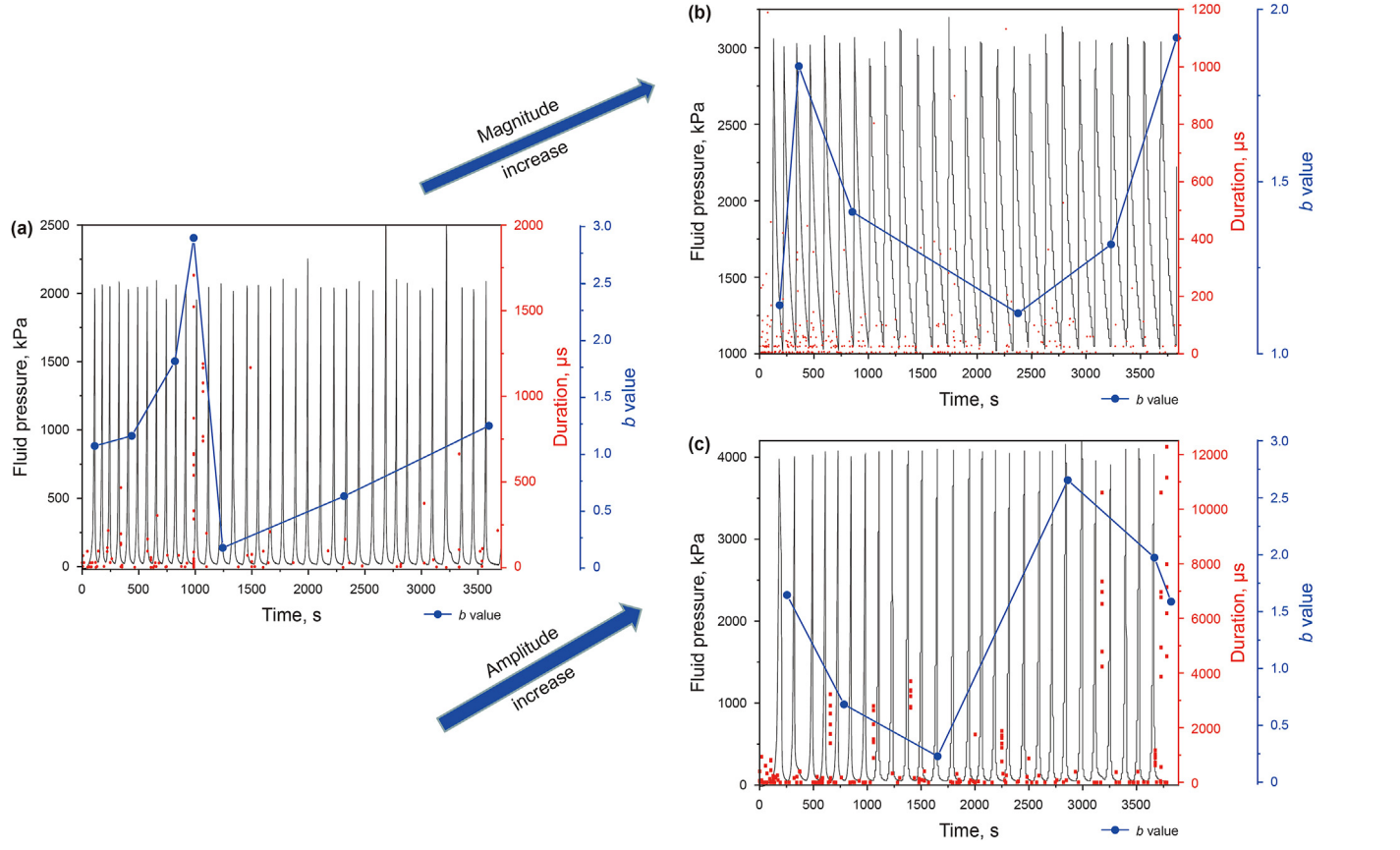

Fig. 12. "N" type of *b* value stimulated with different amplitudes of cycle and magnitudes of fluid pressure by low alternating fluid pressure. The red points in the figure are the duration of AE parameters, the black line is the fluid pressure, and the blue dash-dotted line is the change of b value.

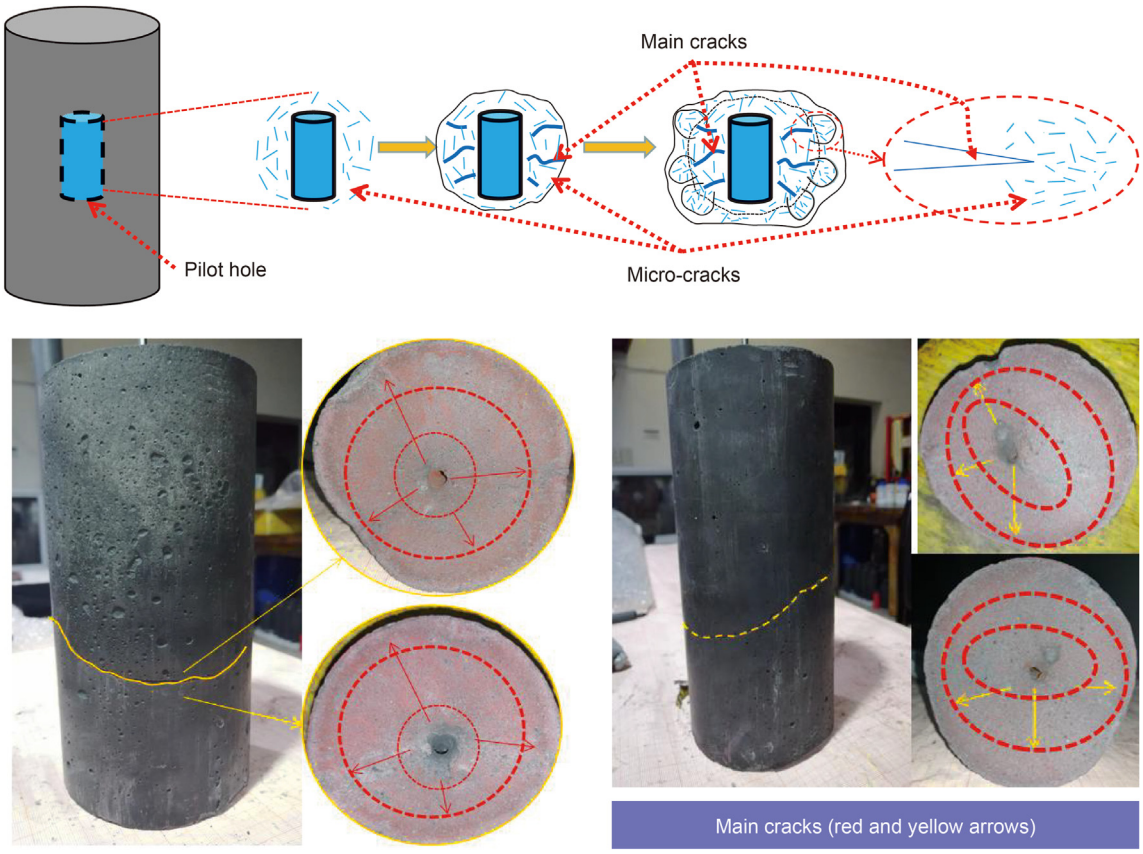

Fig. 13. Damage evolution law of "N" type of *b* value.

express the rock damage process by referring to relevant research on damage mechanics (Unander, 1993), and the *b* value is also used to describe the initiation and propagation of cracks. Specifically, with the increase in the *b* value, the sample is fracturing on a small scale and the proportion of small AE events to total events increases. On the contrary, the sample is mainly fracturing at a large size, and the proportion of large AE events to total events increases with the reduction of the *b* value. If the *b* value is constant, it indicates that the distribution of large and small cracks is uniform, and the proportion of AE events remains unchanged. In this paper, the maximum likelihood estimation (MLE) method (Unander, 1993) was used to calculate the *b* value, and the calculating formula is as follows:

$$b = \frac{n\lg e}{\sum_{i=1}^{n} \lg A_i - n\lg A_{\min}} \tag{16}$$

As shown in Fig. 12, a lot of AE signals are produced (red points) with a long duration during the propagation of main cracks (the *b* value decreases sharply), which shows that the propagation of main cracks will induce more micro-cracks, and then micro-cracks are interconnected to form a new main crack. With the increase in the *b* value, the AE signals are less with a short duration, indicating that new micro-cracks are formed again. With the increases in the amplitude and magnitude of the cyclic fluid pressure, the duration of the first propagation for micro-cracks decreases (the *b* value increases firstly in Fig. 12).

Under the stimulation of lower-value magnitude CSS, the *b* value shows the "N" type (Fig. 12) owing to the damage of crack propagating. The "N" type of *b* value reveals that the small AE events increase firstly, and the micro-cracks begin to form. Then the large AE events increase, and the micro-cracks are interconnected leading to the generation of main cracks. At the end of CSS, the small AE events are increased again, and new micro-cracks are produced. With the lower-value magnitude CSS, the damage of crack propagation is promoted by the two blossoms of micro cracks, and the main cracks are formed and propagated in this process (Fig. 13).

As shown in Fig. 14, the evolution of the *b* value presents a "W" shape under higher-value magnitude CSS. In the initial phase of the higher-value magnitude CSS, the *b* value is reduced, and the main cracks generate. With the continuous effect of the higher-value magnitude CSS, the main cracks propagate to a stable size. And then, the micro-cracks initiate and propagate once again to form the large-scale main crack (Fig. 15). Therefore, based on the "W" type of *b* value, it can see that the propagation of micro-cracks is strengthened and three times the large-scale main crack propagation are present under the higher-value magnitude CSS. In particular, the second propagation of the main crack takes the shortest time, indicating that the skeleton around the crack had been weakened after the first propagation of the main crack, and the propagation rate of the second main crack is larger than that of the first main crack. At the same time, the sample undergoes three times micro-crack propagation processes, and the duration of micro-crack propagation is increased gradually. It can be concluded that the crack propagation in the skeleton is significantly enhanced, and more abundant micro-cracks are generated under the action of higher-value magnitude CSS.

4.2. Effect of CSS on the radiated energy

In the process of CSS, the propagation of micro-cracks and the hydraulic energy are codependent, where the hydraulic energy is introduced by hydraulic fracturing treatments. A part of hydraulic

energy transforms into heat energy and dissipates during the crack propagation, which is called stimulated energy. The other small part is seismic, and it can be detected by the AE sensors and turned into the AE signals, which is called radiated energy (Stoeckhert et al., 2015; Li et al., 2019; Liang et al., 2019; Zhang et al., 2021). Therefore, the radiated energy obtained from the AE signals is the opposite of the dissipation stimulated energy produced during the CSS. Fig. 16 shows that with the increase in the amplitude of cyclic fluid pressure, the radiated energy reduces gradually during the sample is fracturing. Based on the result, the radiated energy is 42797.33 mV ms during the sample is breaking under monotonic hydraulic fracturing, when the amplitude of the CSS is 2 MPa, the radiated energy is larger than 18,000 mV ms, and when the amplitude of the CSS is 4 MPa, the radiated energy is less than 18,000 mV ms (Fig. 16). Thus, the radiated energy can be reduced under the CSS during hydraulic fracturing. The larger the amplitude of circulation stimulation, the more stimulated energy is dissipated during the CSS, and the more conducive to reducing the radiated energy during the sample is breaking. Furthermore, the radiated energy is large under the lower-value magnitude of alternating fluid pressure, while with the higher-value magnitude of alternating fluid pressure, the radiated energy is small. Based on the discussion in Section 4.1, with high cyclic fluid pressure, the fracture process zone of CSS is large, micro-cracks are abundant, and the radiated energy is small. Moreover, the difference of radiated energy under alternating fluid pressure with higher-value magnitudes is smaller than that under alternating fluid pressure with lower-value magnitudes, which shows that more stimulated energy is released during CSS with a higher-value magnitude.

During the CSS, with the multiple increase and decrease of fluid pressure, the micro-cracks in the rock continuously initiate and propagate then to promote the damage evolution of the rock. According to the energy dissipation criterion of damage, the damage variable can be defined as (Attewell and Farmer, 1973; Chen et al., 2017a):

$$D = \frac{e_{\text{eff}}}{e_{\text{tot}}} \tag{17}$$

where e_{eff} is the effective energy during the CSS, and its value equals the stimulated energy; e_{tot} is the total input energy, and it is the hydraulic energy. They can be calculated as follows:

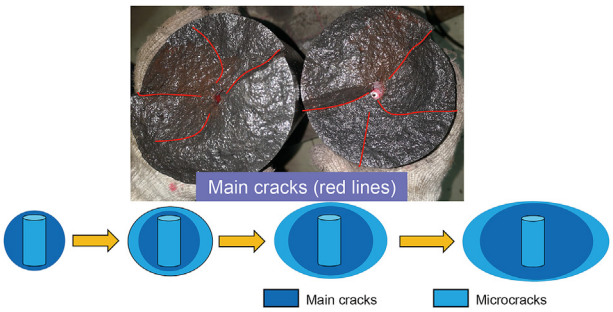

Fig. 15. Damage evolution law of "W" type of *b* value.

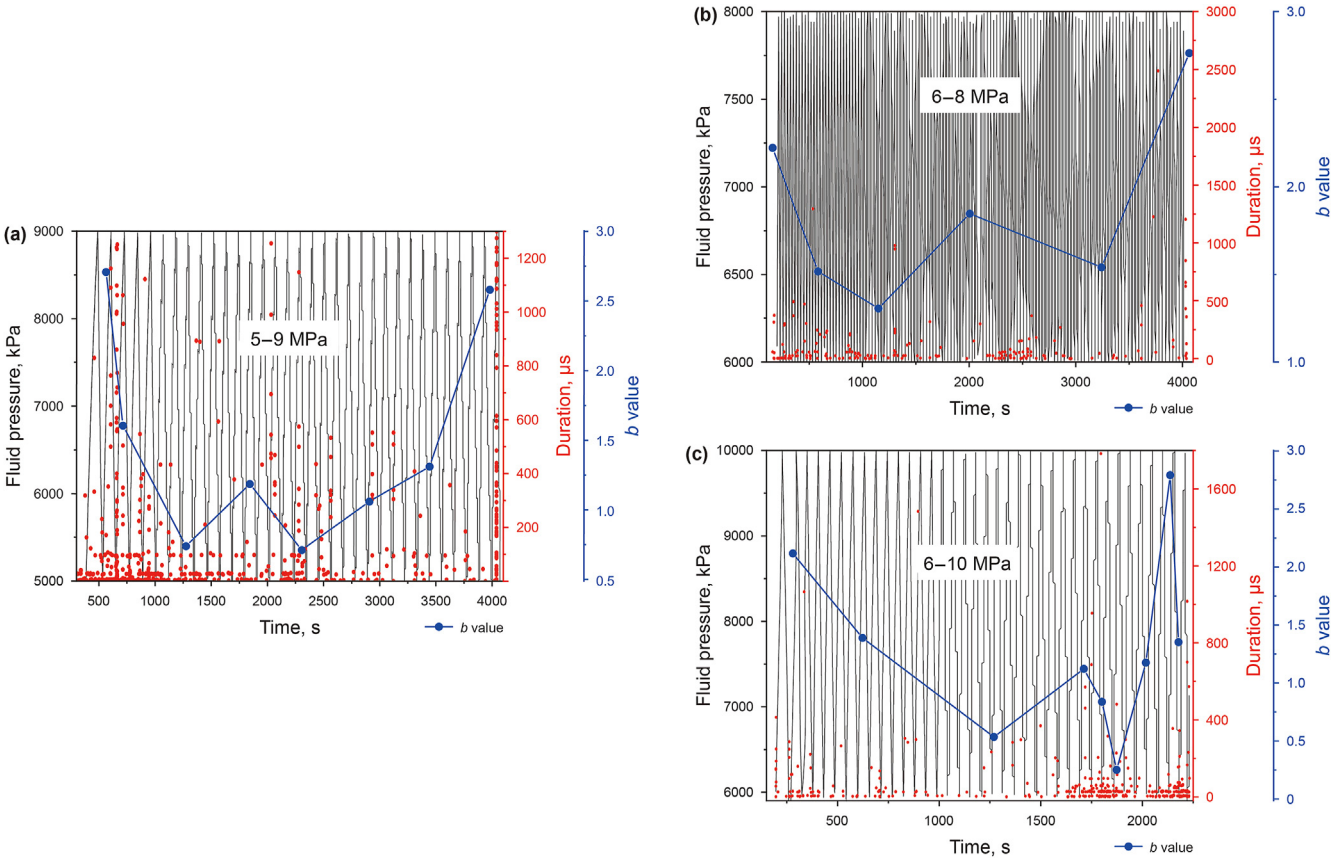

Fig. 14. "W" type of *b* value stimulated by high alternating fluid pressure. The red points in the figure are the duration of AE parameters, the black line is the fluid pressure and the blue dash-dotted line is the change of *b* value.

$$e_{\mathrm{eff}} = \int_{t_0}^{t_1} p_{\mathrm{extend}}^2 \mathrm{d}t = \int_{t_0}^{t_1} \left[9.16\times10^{-2} \cdot \left(x \cdot \frac{\partial L(\Delta t)}{L^2(\Delta t)\partial t} \right) \cdot \Delta P + (1+\alpha)P_{\mathrm{w}} - 3\sigma_3 + \sigma_1 \right]^2 \mathrm{d}t \tag{18}$$

$$e_{\mathrm{tot}} = \int_{t_0}^{t_1} p_{\mathrm{w}}^2 \mathrm{d}t \tag{19}$$

Based on the rock fracture mechanics, the initiation and propagation of cracks are driven by the surface energy *Us*, and the surface energy is consistent with the maximum radiated energy:

$$U_{\mathrm{s}} = 4\gamma C \tag{20}$$

By combining Eq. (18)–Eq. (20), with the stimulation of cyclic fluid pressure, the maximum stimulated energy of the crack propagation reduces to $U_{\mathrm{s}}^{'}$:

$$U_{\mathrm{s}}^{'} = 4\gamma^{'} C = 4C \cdot \gamma \cdot (1-D) \approx 4C \cdot \gamma \cdot \int_{t_0}^{t_1} \left(\frac{3\sigma_3 - \sigma_1 - 9.16\times10^{-2} \cdot \Delta P \cdot (t_1 - t_0) - P_{\mathrm{p}}}{P_{\mathrm{w}}} \right)^2 \mathrm{d}t \tag{21}$$

According to Eq. (21), the relationship between the maximum radiated energy and the alternating fluid pressure is established. It concludes that with the increase in fluid pressure P_{w} and the cyclic amplitude ΔP, the surface energy U_{s} of the crack initiation and propagation reduces. The radiated energy during the sample breaking has a positive correlation with the surface energy of crack U_{s}, which supports the results of Fig. 16. Under high-value cyclic fluid pressure P_{w}, the difference of U_{s} is small. The reason is that the P_{w} is large, and the change of U_{s} with varied cyclic amplitude ΔP is mainly dependent on the P_{w}. Therefore, as for the application of the CSS and the reduction of the maximum radiated energy, the cyclic fluid pressure should be raised properly, and the amplitude of the fluctuating fluid pressure should be increased as much as possible.

5. Conclusions

The purpose of the current study was to investigate the mechanical effects of cyclic fluid pressure with different magnitudes and amplitudes on crack propagation and maximum radiated energy in hydraulic stimulation. Based on the macro-scale experimental results (fluid pressure) and the micro-scale AE analysis (*b* value and radiated energy), the following conclusions can be drawn:

(1) From the macro-scale investigations, lower-value magnitudes of CSS lead to a larger peak value of the fluid pressure, while with the amplitude of CSS increasing, the peak value of fluid pressure decreases. With the increase in the amplitude

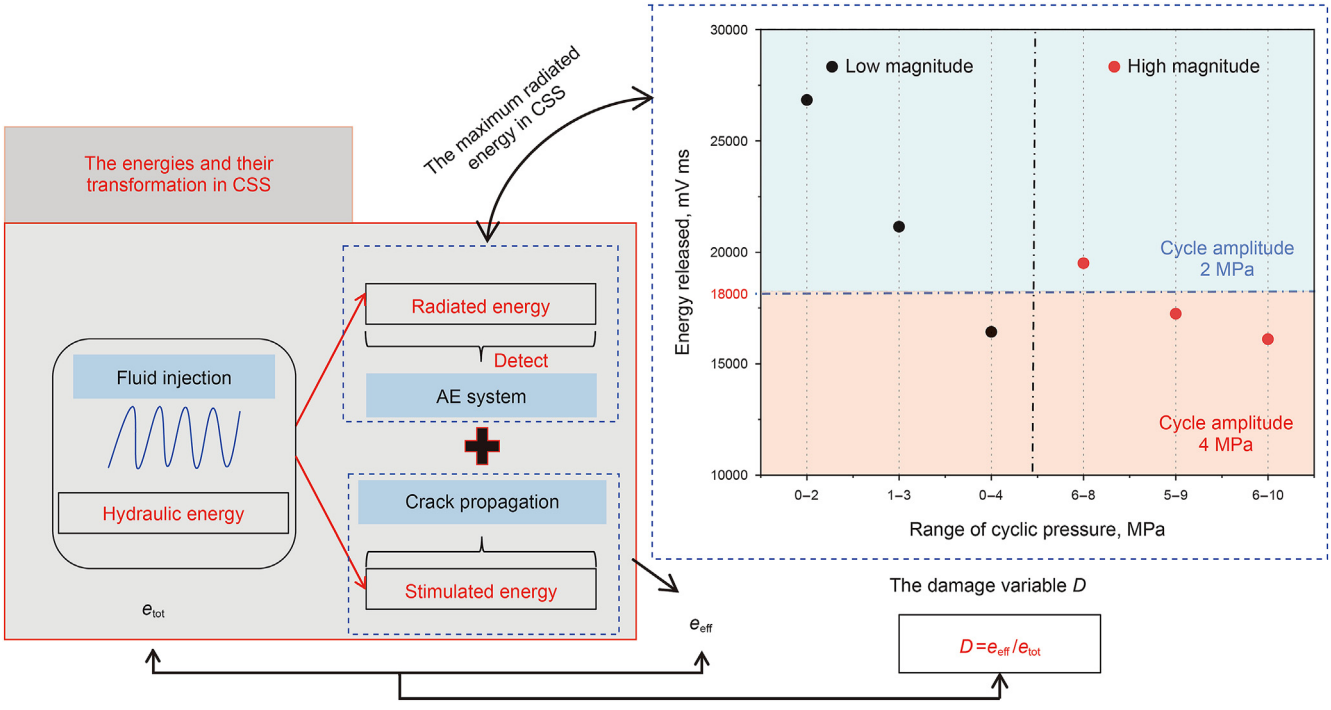

Fig. 16. Maximum released stimulated energy of different CSS. The unit for energy is mV ms, the relative energy is captured by AE; the dash-dotted line is the bound of relative energy for different amplitudes of cyclic fluid pressure, the value is 18,000.

of CSS, the pressurization rate and propagation pressure of crack increase, while the durations of pressurization and crack propagation decrease.

(2) From the micro-scale analysis, it concludes that more abundant micro-cracks are generated under the action of the higher-value magnitude of cyclic fluid pressure. The crack extending criterion has been proposed to link the injection parameters under CSS, the rock properties, and *in-situ* stress. The fluctuation fluid pressure causes the reduction of a critical crack extending pressure, and the CSS causes the crack to initiate and propagate under low fluid pressure. With the increasing depth, the *in-situ* stress is larger, and the fluid pressure or the amplitude of fluctuating pressure should be increased in the field.

(3) The maximum radiated energy decreases with the increase in the amplitude of CSS and the magnitude of alternating fluid pressure. The relationship between MRE and the alternating fluid pressure is established using the damage variable based on the energy dissipation criterion. To reduce the maximum radiated energy, the cyclic fluid pressure should be raised properly, and the amplitude of the fluctuating fluid pressure should be increased as much as possible.

Acknowledgements

The work investigated in this paper was supported by the National Natural Science Foundation of China (Grant No. 41302124, No. 52078494), Open Funding by Hubei Intelligent Geological Equipment Engineering Technology Research Center (Grant No. DZZB202002), Open Funding by Engineering Research Center of Rock Soil Drilling & Excavation and Protection (Grant No. PL202001), and the Independent Innovation Project of Central South University (Grant No. 2019zzts634). We are also grateful to all the editors and reviewers for their invaluable comments.

References

Ali, T.C., Hamid, H.H., Musharraf, Z., Saied, B.Z., 2018. Propagation and aperture of staged hydraulic fractures in unconventional resources in toughness-dominated regimes. J. Rock Mech. Geotech. Eng. 10 (2), 249–258. https://doi.org/10.1016/j.jrmge.2017.08.003.

Antonio, P.R., Luigi, I., Sebastian, H., Flaminia, C., Luca, U., Stefan, W., 2020. Combined approach of poroelastic and earthquake nucleation applied to the reservoir-induced seismic activity in the Val d'Agri area, Italy. J. Rock Mech. Geotech. Eng. 12 (4), 802–810. https://doi.org/10.1016/j.jrmge.2020.04.003.

Atkinson, B.K., Yin, X.C., Xiu, J.G., 1992. Fracture Mechanics of Rock. Seismological Press, Beijing, pp. 242–253.

Attewell, P.B., Farmer, I.W., 1973. Fatigue behaviour of rock. Int. J. Rock Mech. Min. Sci. 10 (1), 1–9. https://doi.org/10.1016/0148-9062(73)90055-7.

Bai, M., Mclennan, J., Guo, Q., 2006. Cyclic Injection Modeling of Cutting Re-injection. The 41st U.S. Symposium on Rock Mechanics, Colorado.

Bao, X., Eaton, D.W., 2016. Fault activation by hydraulic fracturing in western Canada. Science 354 (6318), 1406–1409. https://doi.org/10.1126/science.aag2583.

Cao, H., Gao, Q., Ye, G.Q., 2020. Experimental investigation on anisotropic characteristics of marine shale in Northwestern Hunan, China. J. Nat. Gas Sci. Eng. 81, 103421. https://doi.org/10.1016/j.jngse.2020.103421.

Cao, H., Gao, Q., Bao, T., 2021. Investigation on the time-dependent characterization of stimulation behaviors for the shale under fracturing fluid invading. J. Petrol. Sci. Eng. 200, 108384. https://doi.org/10.1016/j.petrol.2021.108384.

Chao, S., Heng, Z., Wei, D.L., Wenting, L., 2020. Numerical investigation of complex fracture network creation by cyclic pumping. Eng. Fract. Mech. 233, 107103. https://doi.org/10.1016/j.engfracmech.2020.107103.

Chen, J.Z., Cao, H., Sun, P.H., 2017a. Mechanisms of fracture extending in coal rock by pulse hydraulic fracturing under triaxial loading. Rock Soil Mech. 38 (4), 1023–1031. https://doi.org/10.16285/j.rsm.2017.04.013 (in Chinese).

Chen, J.Z., Cao, H., Sun, P.H., 2017b. Evaluation of fracture properties of shale in Niutitang Formation, northwest hunan. Earth Sci. Front. 24 (6), 390–398. https://doi.org/10.13745/j.esf.yx.2017-2-50 (in Chinese).

Chen, J.Z., Li, X.B., Cao, H., 2019. Experimental investigation of coal-like materials for hydraulic fracturing based on fluid-solid interaction. J. Nat. Gas Sci. Eng. 69, 102928. https://doi.org/10.1016/j.jngse.2019.102928.

Diaz, M., Jung, S.G., Zhuang, L., 2018a. Hydraulic, Mechanical and Seismic Observations during Hydraulic Fracturing by Cyclic Injection on Pocheon Granite. The 10th Asian Rock Mechanics Symposium.

Diaz, M., Jung, S.G., Zhuang, L., Kim, K.Y., 2018b. Comparison of Acoustic Emission Activity in Conventional and Cyclic Hydraulic Fracturing in Cubic Granite Samples under Tri-axial Stress State. The 52nd U.S. Rock Mechanics/Geomechanics Symposium. Paper Number: ARMA-06-1021.

Farkas, M., Hofmann, H., Zimmermann, G., 2018. Numerical Investigation of Cyclic Hydraulic Stimulation and Related Induced Seismicity in Pohang Fractured Geothermal Reservoir. The 2nd International Discrete Fracture Network Engineering Conference.

Gao, Q., Cao, H., Tianyi, W., 2019. Experimental of dynamic response of hydraulic fracture characteristic parameters of shale under triaxial loading. Geol. Sci. Technol. Inf. 38 (5), 261–268. https://doi.org/10.19509/j.cnki.dzkq.2019.0528 (in Chinese).

Hofmann, H., Zimmermann, G., Zang, A., 2018. Cyclic soft stimulation (CSS): a new fluid injection protocol and traffic light system to mitigate seismic risks of hydraulic stimulation treatments. Geoth. Energy 6–27. https://doi.org/10.1186/s40517-018-0114-3.

Hofmann, H., Zimmermann, G., Farkas, M., 2019. First field application of cyclic soft stimulation at the Pohang Enhanced Geothermal System site in Korea. Geophys. J. Int. 217, 926–949. https://doi.org/10.1093/gji/ggz058.

Huang, L.K., Liu, J.J., Zhang, F.S., Dontsov, E., Damjanac, 2019. Exploring the influence of rock inherent heterogeneity and grain size on hydraulic fracturing using discrete element modeling. Int. J. Solid Struct. 176–177, 207–220. https://doi.org/10.1016/j.ijsolstr.2019.06.018.

Ingrid, T., Marte, G., 2017. Coupled hydro-thermo-mechanical modeling of hydraulic fracturing in quasi-brittle rocks using BPM-DEM. J. Rock Mech. Geotech. Eng. 9 (1), 92–104. https://doi.org/10.1016/j.jrmge.2016.10.001.

James, P., Verdon, L.S., 2016. Carbon capture and storage, geomechanics and induced seismic activity. J. Rock Mech. Geotech. Eng. 8 (6), 928–935. https://doi.org/10.1016/j.jrmge.2016.06.004.

Lee, K.K., Ellsworth, W.L., Giardini, D., 2019. Managing injection-induced seismic risks. Science 364 (6442), 730–732. https://doi.org/10.1126/science.aax1878.

Lei, Q.H., Wang, X.G., Min, K.B., Rutqvist, J., 2020. Interactive roles of geometrical distribution and geomechanical deformation of fracture networks in fluid flow through fractured geological media. J. Rock Mech. Geotech. Eng. 12 (4), 780–792. https://doi.org/10.1016/j.jrmge.2019.12.014.

Lemaitre, J., Desmorat, R., 2005. Engineering Damage Mechanics: Ductile, Creep, Fatigue and Brittle Failures. Springer, Berlin.

Li, T.T., Pei, X.J., Wang, D.P., Huang, R.Q., Tang, H., 2019. Nonlinear behavior and damage model for fractured rock under cyclic loading based on energy dissipation principle. Eng. Fract. Mech. 206, 330–341. https://doi.org/10.1016/j.engfracmech.2018.12.010.

Liang, T., Guan, B., Yan, Y., 2018a. Laboratory Study of Hydraulic Fracturing in Cyclic Injection. The 52nd U.S. Rock Mechanics/Geomechanics Symposium.

Liang, T.C., Liu, Y.Z., Fu, H.F., Yan, Y.Z., Xiu, N.L., Wang, Z., 2018b. Experimental study of hydraulic fracturing simulation for multistage circulating pump injection. Rock Soil Mech. 39 (S1), 355–361. https://doi.org/10.16285/j.rsm.2017.1834 (in Chinese).

Liang, T.C., Fu, H.F., Liu, Y.Z., Xiu, N.L., Yan, Y.Z., 2019. On the determination method of rupture mechanism in acoustic emission used in hydraulic fracturing fracture propagation. J. Exp. Mech. 34 (2), 358–364 (in Chinese).

Lou, Y., Zhang, G.Q., 2019. Experimental analysis of fracturing fluid viscosity on cyclic hydraulic fracturing. Rock Soil Mech. 40 (S1), 109–118. https://doi.org/10.16285/j.rsm.2018.2256 (in Chinese).

Mateusz, J., Baotang, S., Mikael, R., 2019. Simulation of the interactions between hydraulic and natural fractures using a fracture mechanics approach. J. Rock Mech. Geotech. Eng. 11 (6), 1138–1150. https://doi.org/10.1016/j.jrmge.2019.07.004.

McGlade, C.E., 2012. A review of the uncertainties in estimates of global oil resources. Energy 47, 262–270. https://doi.org/10.1016/j.energy.2012.07.048.

Patel, S.M., Sondergeld, C.H., Rai, C.S., 2017. Laboratory studies of hydraulic fracturing by cyclic injection. Int. J. Rock Mech. Min. Sci. 95, 8–15. https://doi.org/10.1016/j.ijrmms.2017.03.008.

Philip, M.B., David, C.A., Stephan, G., 2020. Laboratory simulations of fluid-induced seismicity, hydraulic fracture, and fluid flow. Geomech. Energy and the Environ. 24, 100169. https://doi.org/10.1016/J.GETE.2019.100169.

Sampath, K.M., Perera, M.S., Ranjith, P.G., 2018. Theoretical overview of hydraulic fracturing break-down pressure. J. Nat. Gas Sci. Eng. 58, 251–265. https://doi.org/10.1016/j.jngse.2018.08.012.

Stoeckhert, F., Molenda, M., Brenne, S., 2015. Fracture propagation in sandstone and shale laboratory experiments,acoustic emissions and fracture mechanics. J. Rock Mech. Geotech. Eng. 7, 237–249. https://doi.org/10.1016/j.jrmge.2015.03.011.

Tan, P., Pang, H.W., Zhang, R.X., Jin, Y., Zhou, Y.C., Kao, J.W., Fan, Meng, 2020. Experimental investigation into hydraulic fracture geometry and proppant migration characteristics for southeastern Sichuan deep shale reservoirs. J. Petrol. Sci. Eng. 184, 106517. https://doi.org/10.1016/j.petrol.2019.106517.

Tong, S.K., Gao, D.L., 2018a. Mechanical principles of hydraulic pressure fluctuation injection based on fracturing technology. Oil Drill. Prod. Tech. 40 (2), 265–274. https://doi.org/10.13639/j.odpt.2018.02.021 (in Chinese).

Tong, S.K., Gao, D.L., 2018b. Analysis of pressure and tip stress in hydraulic fracture under unstable fluid injection condition. China Petrol. Mach. 46 (11), 65–71. https://doi.org/10.16082/j.cnki.issn.1001-4578.2018.11.011 (in Chinese).

Unander, T.E., 1993. The effect of attenuation on b-values in acoustic emission

measurements-A theoretical investigation. Int. J. Rock Mech. Min. Sci. Geomech. Abstracts 30 (7), 947–950. https://doi.org/10.1016/0148-9062(93)90050-N.
Wang, X.H., Zhang, F.S., Tang, M.R., Du, X.F., Tang, J.Z., 2022. Effect of stress shadow caused by multistage fracturing from multiple well pads on fracture initiation and near-wellbore propagation from infill wells. SPE J. 27 (1), 204–225. https://doi.org/10.2118/208577-PA.
Wu, J.J., Shaohe, Z., Cao, H., 2020. Experimental investigation of crack dynamic evolution induced by pulsating hydraulic fracturing in coalbed methane reservoir. J. Nat. Gas Sci. Eng. 75, 103159. https://doi.org/10.1016/j.jngse.2020.103159.
Xie, J.N., Xie, J., Ni, G.H., 2020. Effects of pulse wave on the variation of coal pore structure in pulsating hydraulic fracturing process of coal seam. Fuel 264, 116906. https://doi.org/10.1016/j.fuel.2019.116906.
You, M., 2015. Strength criterion for rocks under compressive-tensile stresses and its application. J. Rock Mech. Geotech. Eng. 7 (4), 434–439. https://doi.org/10.1016/j.jrmge.2015.05.002.
Zang, A., Yoon, J.S., Stephansson, O., 2013. Fatigue hydraulic fracturing by cyclic reservoir treatment enhances permeability and reduces induced seismicity. Geophys. J. Int. 195 (2), 1282–1287. https://doi.org/10.1093/gji/ggt301.
Zang, A., Zimmermann, G., Hofmann, H., Stephansson, O., 2019. How to reduce fluid-injection-induced seismicity. Rock Mech. Rock Eng. 52, 475–493. https://doi.org/10.1007/s00603-018-1467-4.
Zhang, Z.B., Liu, X.N., Zhang, Y.H., Qin, X.Y., Khan, M., 2021. Comparative study on fracture characteristics of coal and rock samples based on acoustic emission technology. Theor. Appl. Fract. Mech. 111, 102851. https://doi.org/10.1016/j.tafmec.2020.102851.
Zhou, Z., Zhang, G.Q., Xing, Y.K., 2019. A laboratory study of multiple fracture initiation from perforation clusters by cyclic pumping. Rock Mech. Rock Eng. 52 (3), 827–840. https://doi.org/10.1007/s00603-018-1636-5.
Zhuang, L., Kim, K.Y., Jung, S.G., 2018. Cyclic Hydraulic Fracturing of Cubic Granite Samples under Triaxial Stress State with Acoustic Emission, Injectivity and Fracture Measurements. The 52nd U.S. Rock Mechanics/Geomechanics Symposium.
Zhuang, L., Kim, K.Y., Jung, S.G., Diaz, M., Min, K.B., 2019. Effect of water infiltration, injection rate and anisotropy on hydraulic fracturing behavior of granite. Rock Mech. Rock Eng. 52, 575–589. https://doi.org/10.1007/S00603-018-1431-3.
Zimmermann, G., Moeck, I., Blöcher, G., 2010. Cyclic water fracturing stimulation to develop an Enhanced Geothermal System (EGS)-conceptual design and experimental results. Geothermics 39 (1), 59–69. https://doi.org/10.1016/j.geothermics.2009.10.003.
Zimmermann, G., Hofmann, H., Babadagli, T., 2015. Multi-fracturing and Cyclic Hydraulic Stimulation Scenarios to Develop Enhanced Geothermal Systems-Feasibility and Mitigation Strategies to Reduce Seismic Risk. The World Geothermal Congress.